

Preparation of Tin-doped Carbon Hollow Spheres and Their Electrocatalytic activity in Water Electrolysis

Jayeeta Chattopadhyay*, Rohit Srivastava, P.K. Srivastava

Department of Applied Chemistry, Birla Institute of Technology, Deoghar Extension campus Jasidih – 814 142, Jharkhand, India

*E-mail: jayeeta08@gmail.com

Received: 17 December 2012 / Accepted: 21 January 2013 / Published: 1 March 2013

Hollow carbon sphere electrocatalysts were synthesized by combining the hydrothermal and intermittent microwave heating (IMH) technique. The addition of P123 as surfactant has created huge amount of pores, resulted in the ultrahigh surface area of $1300 \text{ m}^2 \text{ g}^{-1}$. The formation of rutile SnO_2 phase during tin loading over spherical structure has enhanced the electrocatalytic activity of the materials towards hydrogen and oxygen evolution reaction from water electrolysis in acidic media. The SEM and TEM images have confirmed the hollow spherical structure with the diameter of 300 – 400 nm. The XRD pattern and micrographs have shown the formation of SnO_2 phase. The nitrogen adsorption isotherm has exhibited typical type – I of microporous materials. In the cyclic voltammograms, the peaks for hydrogen and oxygen evolution reactions are prominent in all the electrocatalysts. Among all the electrocatalysts, 30 wt% Sn/HCS – 6 has shown the best electrocatalytic activity with 30 and 50 mA.cm^{-2} of cathodic and anodic peak current density value, respectively. The reaction mechanism of the water electrolysis system has exhibited the average reaction order value of -1.16 with Tafel slope of 64 mV.

Keywords: Hollow Carbon Spheres, Electrocatalysts, Tin, Intermittent microwave heating, Hydrogen and Oxygen production

1. INTRODUCTION

Hydrogen is the most common chemical element on the earth, which does not exist largely in its gaseous form. It is required to be extracted from hydrogen containing compounds, e.g., by electrolysis of water or by various thermo-chemical processes from hydrocarbons or other hydrogen carriers. Water resources on earth are so abundant that there will never be any scarcity; thus it is not strange that there is an increasing interest in water electrolysis. Now-a-days, researchers are considered the electrocatalytic hydrogen evolution on various electrode and electrocatalyst materials with

minimization of Pt metal loading on them, as the important challenge during the electrolysis. Although the main purpose of water electrolysis is to obtain hydrogen, but O_2 evolution is the most common anodic reaction coupled with most of the cathodic processes, which is an unavoidable side reaction in many anodic processes [1].

Nanostructured materials have attracted steadily growing attention due to their unique applications relative to their bulk counterparts [2]. These days, there have been immense efforts in the fabrication of colloidal nano-materials with tailored structural, physical, and surface properties [3]. Hollow structures always provide some advantages over their solid counter parts in industrial applications, e.g., fillers, pigments, and coatings, due to their lower density [4 – 8]. Moreover, the optical, electrical, thermal, mechanical, magnetic and catalytic properties of the hollow nanostructures can be tailored in a controllable way over a wide range by manipulating not only the size, shape, and composition of the materials, but also the shell structure including the thickness, porosity, and surface derivatization [9]. The different structures or shaped carbon materials such as onion-like carbon [10], flower-like carbon [11], straw-like carbon [12] and nanorods carbon [13] have been of continuous research interest these days. The hollow carbon spheres (HCSs) are good candidates as catalyst supports due to their high surface area and large pore volume [14]. There are various methods to synthesize HCSs e.g. template [15], pyrolysis [16], reduction [17] and hydrothermal [18]; although these methods are time-consuming and complicated to execute. In the present work, we have adopted an intermittent microwave heating (IMH) technique to prepare hollow carbon spheres, which was earlier mentioned by Wu et al [19]. In this method, HCSs were synthesized using polystyrene (PSs) as template materials along with the glucose decomposition in a poly(ethylene glycol)-block-poly(propylene glycol)-block-poly(ethylene glycol) (P123) surfactant containing solution under hydrothermal condition. During the IMH treatment, trapped P123 molecules have been removed, resulting in the formation of large amount of nanopores and open nanochannels formed on the walls of HCSs. Later, we have doped tin particles over the HCSs, and Sn/HCSs were investigated as the electrocatalysts in hydrogen and oxygen evolution reaction during water electrolysis. In our previous studies, we have reported tin-doped titania hollow spheres as electrocatalysts in hydrogen and oxygen production during water electrolysis [20]. The electrocatalytic activity was considerable enhanced by the tin doping over the titania hollow sphere. SnO_2 has always been considered as dispersing material and also for the enhancement of electrochemical stability of the catalysts. In reality, SnO_2 itself is a semiconductor, which can induce the conductivity of the catalyst surface to a great extent. Zhang et al have synthesized tin nanoparticles encapsulated elastic hollow carbon spheres with uniform size, and have potentially applied in lithium batteries [21]. In the present work, we have loaded tin particles over the hollow carbon spheres and evaluated their electrocatalytic properties in water electrolysis process in acidic media.

2. EXPERIMENTS

2.1. Preparation of HCSs and Sn/HCSs catalysts:

Polystyrene spheres (PSs) were utilized as the template materials to synthesize hollow carbon spheres. Polystyrene sphere were obtained by emulsifier-free dispersion polymerization of styrene

[22]. The requisite amount of glucose (1 mol L^{-1}) (Aldrich, Germany) and 25 wt% PS in P123 (Aldrich, USA) containing solution (2 ml , 50 mg ml^{-1} P123) were added into a 50 ml autoclave and heated at $180\text{ }^{\circ}\text{C}$ for 12 h . The deposited material was washed with ethanol and distilled water and then dried at $80\text{ }^{\circ}\text{C}$ for 2 h . Subsequently, the product was heated in a microwave oven (1400 watt , 50 Hz) by the IMH method by heating for 2 min , followed by 1 min pulse, and heating for 2 , 3 and 4 min . The total heating time for the samples will be 4 , 5 and 6 min , respectively. The first step of the present synthesis method is the mixing of glucose and PS in presence of P123 prior to the hydrothermal reaction, during which PS/carbon core-shell structure is formed. Simultaneously, the P123 molecules are trapped inside the carbon layers. In the final step, IMH treatment in air atmosphere is resulted in the removal of PS with P123 molecules, leaving the large amount of open micropores and nanochannels.

In the present work, tin was loaded over the hollow carbon spheres using SnCl_2 as the precursor material. 10 , 20 and $30\text{ wt}\%$ of Sn/HCSs materials were synthesized by the reduction of SnCl_2 aqueous solution using formic acid as the reducing agent. The mixture was put together into a microwave oven (1500 W , 2.45 GHz , Samsung, Korea) and heated the mixture with IMH method at six intervals of heating for a period of 30 s and pausing for a period of 60 s . The HCS materials with total heating time of 4 , 5 and 6 min has been denoted as HCS – 4, HCS – 5 and HCS – 6, respectively.

2.2. Electrochemical cell preparation and electrochemical characterizations:

The HCSs powder is mixed with Nafion solution (Dupont, 5% solution, equivalent 110 g/mol) and solvent (water and isopropyl alcohol) under sonicating water bath for 20 min for catalyst ink preparation. The catalyst ink is casted onto water-proofed carbon cloth ($1\text{ cm X }1\text{ cm}$), dried at $70\text{ }^{\circ}\text{C}$ in air for removing solvent. The Sn/HCSs loading on the carbon cloth is controlled to 3 mg/cm^2 . All the electrochemical measurements were performed in a three-electrode cell with Potentiostat/Galvanostat (Princeton Applied Research, Parastat® 4000) using Ag/AgCl in 3.5 M KCl solution as reference electrode and Pt plate ($1\text{ cm X }1\text{ cm}$) as counter electrode in $0.1\text{ N H}_2\text{SO}_4$ solution. The cyclic voltammetric measurements were performed in the potential range of -1.2 to 2.0 V with a scan rate of 40 , 80 and 100 mV s^{-1} . The anodic polarization and Tafel slopes were recorded with a potential scan rate of 0.5 mV s^{-1} .

2.3. Physical characterization of HCSs and Sn/HCSs:

The HCSs and Sn/HCSs materials are characterized by an X-ray diffractometer using a D/MAX – 3C equipment of Rigaku Denki Co. Ltd. by using $\text{Cu K}\alpha$ radiation with fixed powder source (30 kV , 15 mA); the applied scan rate was 2° (2θ)/min. BET Surface area of all the spherical materials is measured with Micromeritics ASAP equipment, model 2010 using N_2 adsorption-desorption isotherms at 77.35 K . The thermogravimetric analysis (TGA) was studied using Shimadzu TGA-50H apparatus, by heating the samples up to $700\text{ }^{\circ}\text{C}$ with the $10\text{ }^{\circ}\text{C/min}$ heating rate under air atmosphere (25 ml/min). The surface morphologies of the hollow sphere samples were measured using scanning

electron microscope (SEM) and transmission electron microscope (TEM) with JSM-6400 and JEM-2010, respectively.

3. RESULTS AND DISCUSSIONS

3.1. XRD Analysis:

The XRD patterns of various Sn/HCSs samples with different heat treatment duration, and the composition of tin loading over hollow carbon spheres are presented in Fig. 1 and Fig. 2, respectively.

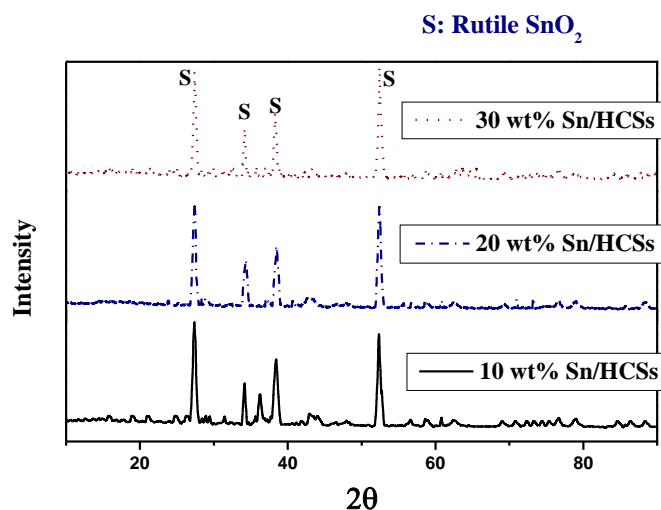


Figure 1. XRD Patterns of 10, 20 and 30 wt% Sn/HCS-6 electrocatalysts

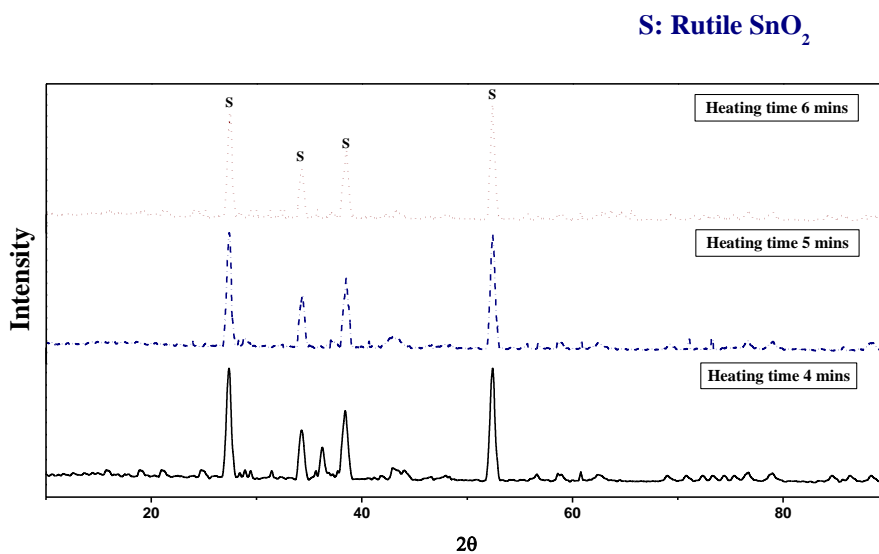


Figure 2. XRD Patterns of 20 wt% Sn-doped HCS with 4, 5, and 6 mins heating time

The results illustrate the presence of tetragonal rutile SnO₂ phase in all the hollow sphere samples. The diffraction peaks around 27°, 34°, 38°, and 52° are found in XRD patterns of all the Sn/HCSs samples, which are ascribed to (111), (101), (200) and (211) planes of tetragonal rutile SnO₂ structure [23 – 25]. The critical growth of SnO₂ phase on the HCSs surface with IMH treatment with longer duration has implied the higher intense peak in the 20 wt% Sn/HCS sample with 6 min heat treatment (Fig. 1). Similarly, Fig. 2 has represented the gradual increase in the peak intensity with the rise in the tin loading over HCSs structure, which can be concluded into the formation of SnO₂ on the surface of the spheres.

3.2. TGA Study

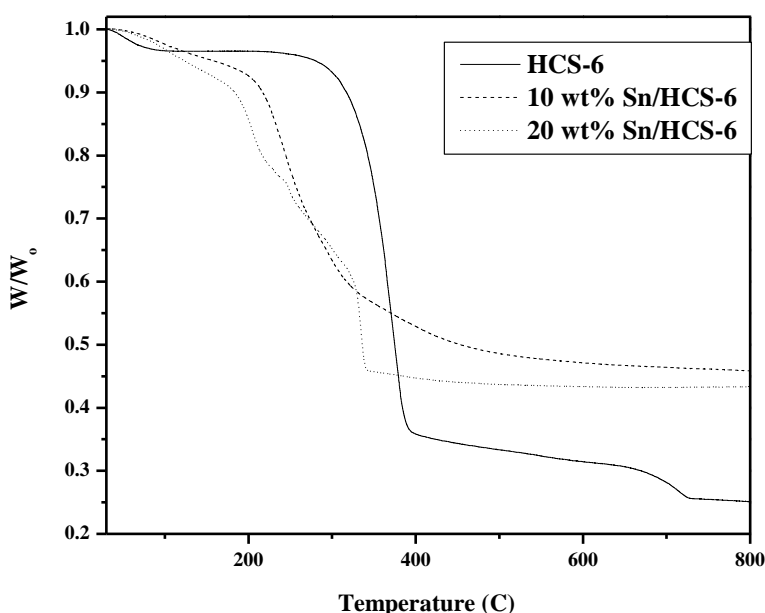


Figure 3. TG Study of 0, 10 and 20 wt% Sn-doped HCSs

Thermogravimetric curves of 0, 10 and 20 wt% HCS-6 electrocatalysts are showing in Fig. 3. The thermal analysis was carried out by heating the materials up to 800 °C at the heating rate of 10 °C/min. It is seen from the results that, the trend of the thermal degradation has changed with tin loading over hollow carbon spheres. The rapid weight loss has started at 292 °C for undoped HCSs material, whereas it is shifted to 200 °C and 178 °C for 10 and 20 wt% Sn-doped HCSs electrocatalysts, respectively. The initial degradation of weight might be attributed to the water evaporation from the catalyst, which was further proceeded into burning out of organic residues, viz. PS and P123 surfactant. The shifting of the initial rapid degradation temperature to lower range for metal doped sample can be explained as the presence of more moisture in those samples; the physically and chemically bound water molecules were evaporated between 150 – 220 °C temperature. The residues are more for the doped catalysts at the final range of temperatures, due to the presence of undecomposed SnO₂. Thermal studies of the entire carbon hollow sphere sampler have confirmed the

thermal stability of the materials. It has also ensured the hollow structure of the catalysts after calcinations, as all the organic residues have burned out during heating.

3.3. BET Surface Area and N₂-Adsorption Isotherm

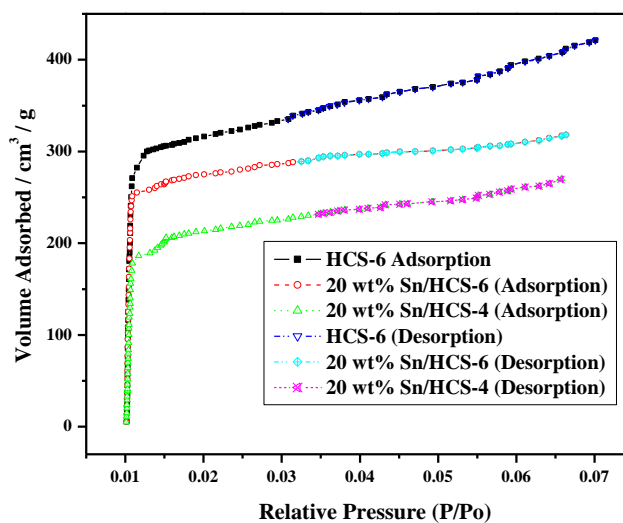


Figure 4. N₂-Adsorption Isotherms of HCS – 6, 20 wt% Sn/HCS – 4 and 20 wt% Sn/HCS – 6

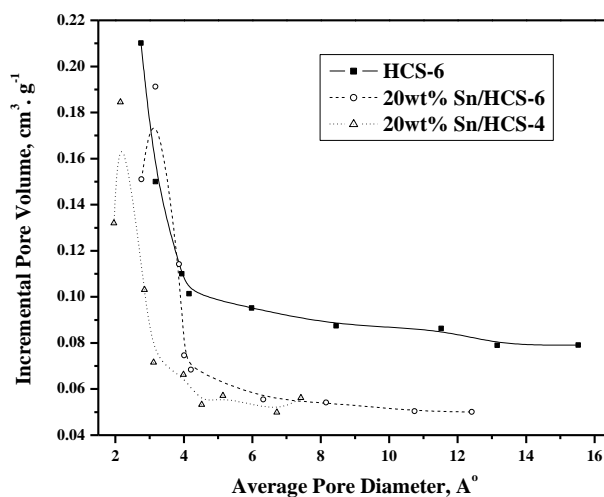


Figure 5. Pore Size Distributions of Sn-doper HCSs

BET surface area and average pore diameter values of with and without doped HCSs materials were analyzed and summarized in Table 1. The surface area value of only hollow carbon sphere with 6 min heating time is revealed as 1300.2 m² g⁻¹, which seems to be a material with an ultrahigh surface area value. On the other hand, the surface areas of tin-doped HCSs materials with various heating time are presenting reduced values with considerable amount, although they all can still be considered as the materials with ultrahigh surface area values. Fig. 4 shows the N₂ adsorption isotherm curves for

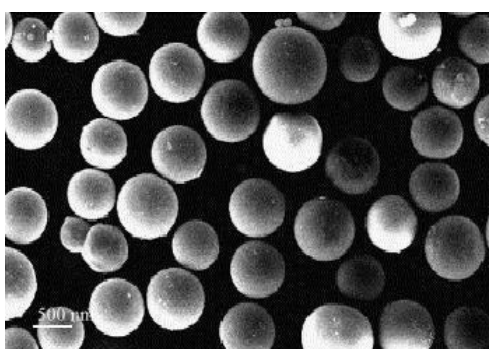
HCS-6, 10wt% Sn/HCS-6 and 20 wt% Sn/HCS-6, which all are exhibiting typical type-I isotherm curves.

Table 1. BET Surface area and pore size results of Sn-doped HCSs electrocatalysts

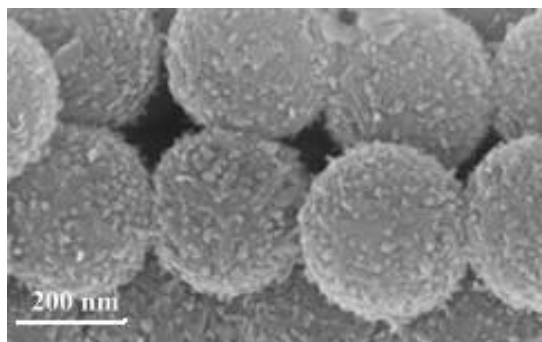
Sample	BET Surface Area (m ² g ⁻¹)	Langmuir Surface Area (m ² g ⁻¹)	Average Pore Diameter (4V/A) (nm)	BJH Adsorption Average Pore Diameter (4V/A) (nm)
HCS-6	1300.2	1351.5	0.625	0.598
10 wt% Sn/HCS-6	1012.4	1075.4	0.432	0.421
20 wt% Sn/HCS-6	1055.4	1101.2	0.429	0.420
30 wt% Sn/HCS-6	1056.1	1099.7	0.422	0.416
20 wt% Sn/HCS-4	819.1	876.2	0.399	0.387
20 wt% Sn/HCS-5	920.6	981.3	0.411	0.407

The micropores formation on the hollow carbon spheres are confirmed with the overlapping of the adsorption and desorption curves in the Fig. 4 for with and without doped HCSs materials. It can be concluded that, tin doping has reduced the surface area of hollow carbon spheres with average pore diameter values. The average pore diameter value of HCS-6 is 0.625 nm, whereas those of 10, 20 and 30 wt% HCS-6 samples exhibited the values of 0.432, 0.429, and 0.422 nm, respectively. It is clear from the BET surface area values and N₂ adsorption curves that, the addition P123 has created huge amount of pores over the spherical surface, and also increase the pore size, resulted in the ultrahigh surface area. Although tin loading over the spheres has blocked the pores to some extent with decrease in the pore diameter, representing reduced surface area values for these samples. Typical pore size distribution for the HCS – 6, 20 wt% Sn/HCS – 4 and 20 wt Sn/HCS-6 electrocatalysts are shown in Fig. 5. Pore size distribution of the prepared HCS – 6 is uniform with the average pore diameter mainly centered at around 0.625 nm. On the other hand, 20 wt% Sn/HCS – 4 and HCS – 6 electrocatalysts have shown a broaden peak around 0.25 and 0.35 nm, respectively; although the curves are extended further in the larger pore size region. The modification in the pore size and structure with the metal loading has been confirmed from pore size distribution results.

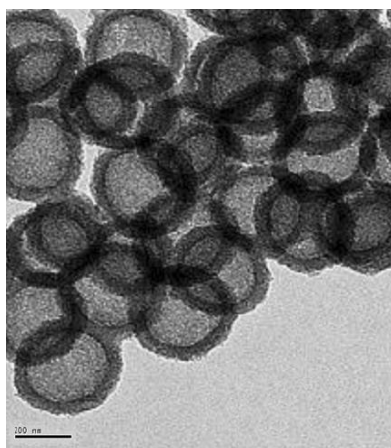
3.4. SEM and TEM Analysis:



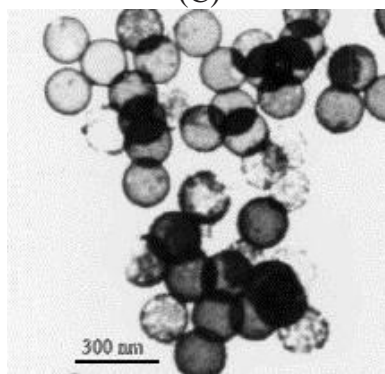
(A)



(B)

Figure 6. (A) and (B): SEM Images of HCSs and Sn-doped HCSs

(C)



(D)

Figure 6. (C) and (D): TEM Images of HCSs and Sn-doped HCSs

Fig. 6 (A) and (B) are showing the SEM images of HCS – 6 and 30 wt% Sn/HCS – 6 electrocatalysts; whereas the TEM images of these hollow sphere samples are represented in 5 (C) and (D). Diameter of all the electrocatalysts were found in the range of 300 – 400 nm. The micrograph images of tin-doped samples have confirmed the formation of SnO₂ over the hollow carbon spheres. We can correlate the coverage of SnO₂ phase with electrochemical characterization results, as the hollow sphere electrocatalysts with greater tin loading has shown better electrocatalytic activity.

3.5. Cyclic Voltammetry:

The Cyclic voltammograms for water electrolysis in acidic media on the hollow carbon sphere with and without loading of tin at different heat treatment duration in microwave assisted system are presented in Fig. 7 and 8 using Ag/AgCl in 3.5 M KCl solution as reference electrode and Pt plate (1cm X 1cm) as counter electrode with the scan rate of 100 mV s^{-1} . In the curves, one anodic (desorption) and cathodic (adsorption) peaks (a_1 and a_2), respectively can be distinguished in the tin-doped HCS samples considering the hydrogen adsorption-desorption reaction.

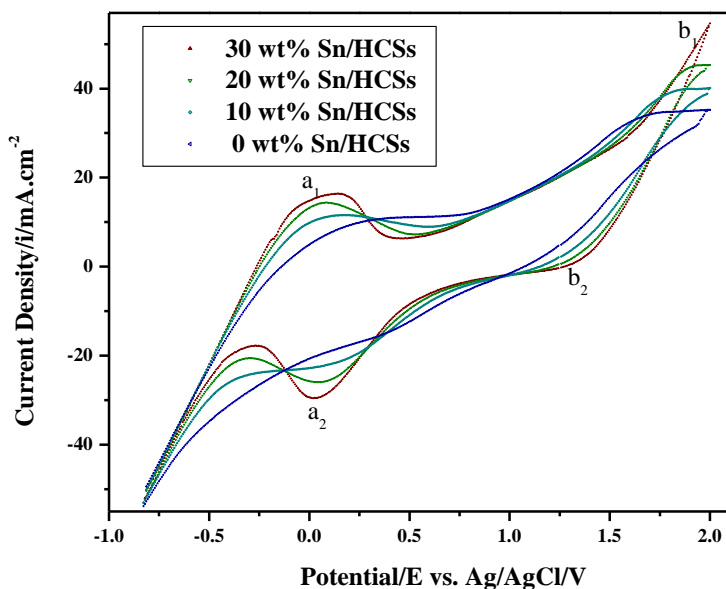


Figure 7. Cyclic Voltammograms of 0, 10, 20 and 30 wt% Sn-doped HCS-6 Electro catalysts

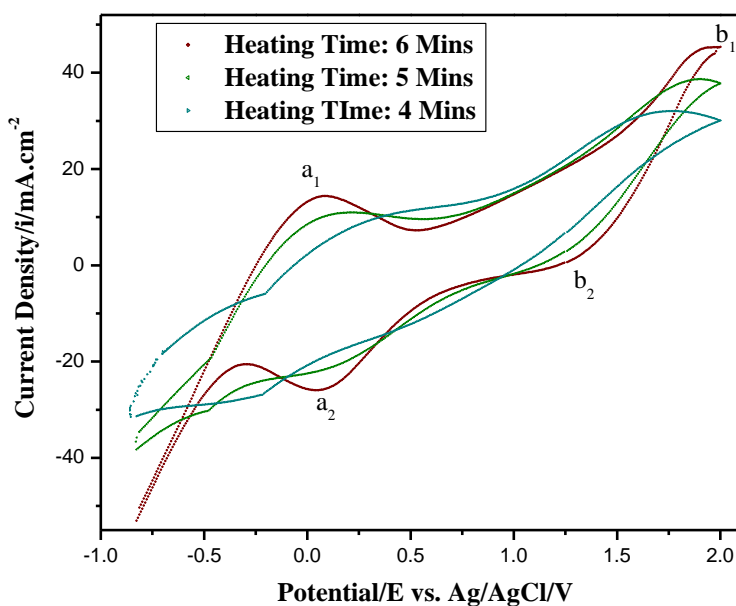


Figure 8. Cyclic Voltammograms of 20 wt% Sn-doped HCS-4, HCS-5 and HCS-6 Electro catalysts

On the other hand, one anodic peak (b_1) has been appeared at 2.0 V, assigned for the oxygen evolution reaction. Similarly, one single peak (b_2) during cathodic sweep attributed to the oxygen reduction (at 1.3 V) is also observed in the 20 and 30 wt% Sn/HCS-6 electrocatalysts; which is faded away with decrease in the tin loading and also with shorter heating duration. In the hydrogen desorption region, the anodic peak a_1 is considered in the literature due to the hydrogen desorption from the bulk of the metal together with desorption of hydrogen adsorbed on the surface [26, 27]. It is resulted in the formation of less intense a_1 peak for pure HCSs (without loading of tin) sample, as the hydrogen adsorbed only on the surface of the hollow sphere (without metal counterpart) has been desorbed in pure HCSs sample. On the other hand, this hydrogen desorption peak becomes more intense with greater tin loading over HCSs material. The similar phenomena happened in the case of a_2 peak, which is assigned for hydrogen gas evolution reaction. The CV results (shown in Fig. 7) are showing that, 30 wt% Sn/HCS-6 can be considered as the best electrocatalysts in this regard; the electrocatalytic activity has been reduced considerably with decrease in the tin loading. Similarly, Fig. 8 presents the 20 wt% Sn-doped HCS samples with heating duration of 4, 5 and 6 mins; which has confirmed the formation of lesser intense a_2 peak in voltammograms with the samples with shorter duration of microwave treatment. On the other hand, 30 wt% Sn/HCS-6 electrocatalyst has produced highest anodic peak current density of $55 \text{ mA}\cdot\text{cm}^{-2}$ (at b_1); this value followed the descending trend in the sample with lesser loading of tin, and reached lowest value of $35.5 \text{ mA}\cdot\text{cm}^{-2}$ with the hollow carbon sphere electrocatalyst without tin loading (HCS-6). Similarly, 30 wt% Sn/HCS-6 electrocatalyst has shown most intense a_2 peak with 30 mA cm^{-2} cathodic peak current density, which is assigned for hydrogen evolution reaction. In the same context, similar trend has been followed with descending order of heating time (Fig. 8). Thus, the electrochemical activity regarding hydrogen and oxygen production has clearly been increased with greater loading of tin over hollow carbon spheres and also with longer heating time, resulting from the intense growth of rutile SnO_2 phase on the surface of the HCSs.

The surface studies and voltammetric studies of hollow carbon spheres have revealed that, the materials with more intense rutile SnO_2 phase are better in hydrogen and oxygen evolution reaction. The similar trend has also been followed in desorption reaction of adsorbed hydrogen during anodic sweep. Although peaks assigned for oxygen and hydrogen production are quite prominent in the cyclovoltammogram for HCS-6 sample. It means the hollow spherical structure of carbon and formation of rutile SnO_2 , both have contributed in the excellent electrocatalytic nature of the samples. Earlier it is reported by many researchers that, hollow carbon spheres exhibit similar behavior like graphite and fullerene; graphite and fullerene are well-known for their oxygen adsorption characteristics [28]. At the same time, SnO_2 is oxygen deficient in nature, thus oxygen vacancies could be created on the surface of the material, especially on the (110) phase of SnO_2 formed over the spherical structure; similarly, it shows strong adsorption property towards hydrogen [29]. Therefore, great extent of hydrogen and oxygen are adsorbed over the large surface of hollow sphere, also to some extent into the void sphere created inside spherical structure. As we can notice that, BET surface area value, intensity of rutile SnO_2 phase and electrocatalytic activity of the hollow carbon spheres samples have shown inclining order with increase in the tin loading over spherical structure, and also with the longer heating time. It means, larger surface area and critical growth of the rutile SnO_2 structure have greatly induced the electrocatalytic behavior of the materials. Usually, on

semiconductor oxides adsorption and diffusion phenomena of oxygen are generated due to oxygen vacancies; in this case, these vacancies are created over spherical structure. The oxygen adsorption at the vacancies resulted in the charge shifting and alteration at the local electronic structure. Moreover, oxygen reduction phenomenon of oxides creates more oxygen vacancies on the surface. During the cathodic potential sweep, reduced species Sn^{2+} ions produced more on the hollow sphere surface, which interact with oxygen, leading to the partial oxygen reduction at a sufficiently large cathodic potential. Usually catalyst surface consist plenty of Sn^{4+} ions, thus oxygen molecules always compete for the more reduced metal ions sites, as they act as electron excess sites. Therefore, oxygen molecules unsymmetrically attached to the metal ions, only one atom bonded to the surface, resulting in the oxygen reduction. This oxygen reduction phenomenon has been proceeded the hydrogen evolution reaction during the cathodic sweep.

3.6. Tafel Lines:

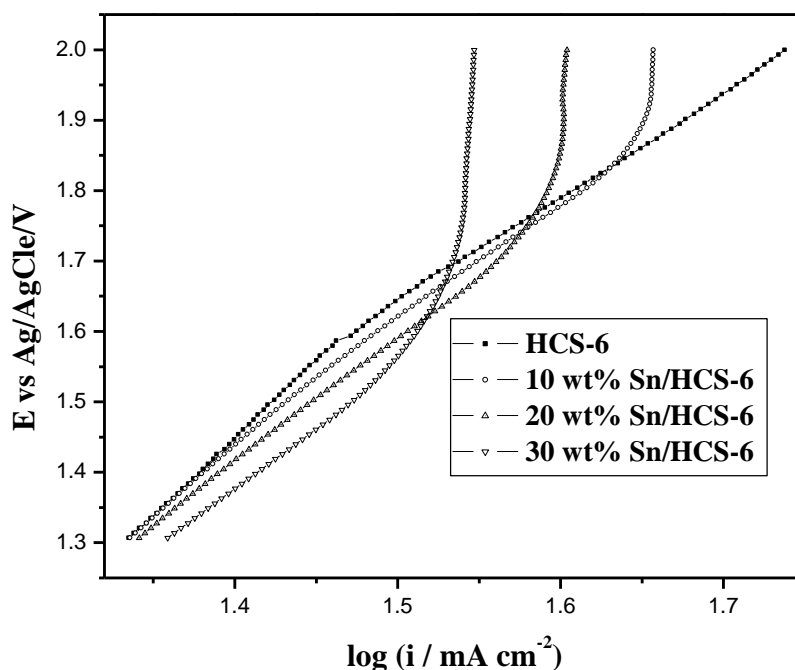


Figure 9. Tafel Plots for O_2 Evolution on 0, 10, 20 and 30 wt% Sn-doped HCS-6 Electrocatalysts

Fig. 9 represents the semilogarithmic plots of potential vs. current density (Tafel plots). The electrocatalytic activity of the hollow carbon sphere materials is showing increasing order with greater loading of metal at lower current density range. The potential at lower current density range is used to exhibit the electrocatalytic performance of the samples without the influence of ohmic resistivity and bubble formation; thus the overpotential generated will only be contributed by the anode reaction. In the higher current density range, the curves are showing appreciable differences, which are mainly affected by ohmic resistance and bubble formation at the support. In this case, the electrocatalytic

performance has been induced by the tin loading, which is also related to the higher surface area value. Tafel slope can be calculated objectively from the Tafel equation which includes uncompensated ohmic drops:

$$E = a + b \ln I + IR \quad (1)$$

After differentiating Eqn. (1) with respect to I will produce:

$$dE/dI = b/I + R \quad (2)$$

Thus, the plot of $\Delta E/\Delta I$ vs. $1/I$ gives the straight line having slope b and intercept of R . Using this equation the average value of Tafel slope is 64 mV.

3.7. Reaction Order:

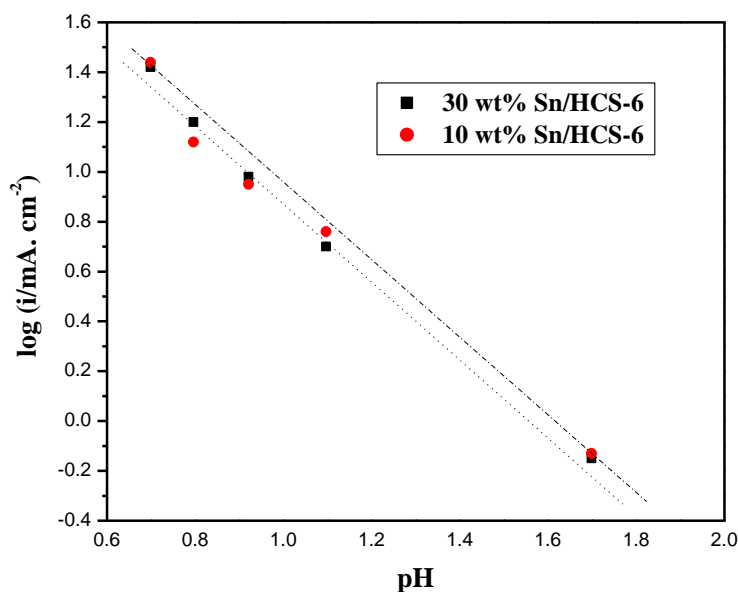


Figure 10. Determination of reaction Order with respect to H^+ for O_2 Evolution at $E = 1.5$ V on 10 and 30 wt% Sn-doped HCS-6 Electro-catalysts

Fig. 10 is showing the typical plot of $\log I$ at $E = 1.5$ V vs. pH for 10 and 30 wt% Sn-doped HCS-6 electro-catalysts. The slope of the straight lines will present the reaction order of the system with respect to the H^+ concentration. The average value of -1.16 has been revealed as the reaction order of the system irrespective of the tin loading and heating duration in the synthesis of hollow sphere materials. Fig. 11 represents the reaction order of all the systems.

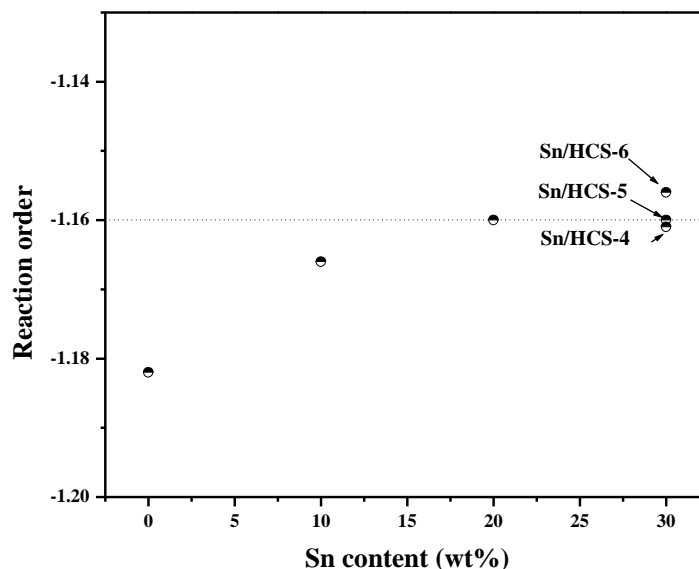


Figure 11. Reaction Order with respect to H^+ for O_2 Evolution on Various HCSs Electrocatalysts with and without doping of Tin

In acidic solution, water molecules are the main reacting particles in oxygen evolution reaction. Thus, the first step of the reaction is:



This step of the reaction can't be the r.d.s., as it would be so, then the reaction order would be zero with respect to H^+ . The possible mechanism of the system would be a chemical step following reaction (3), which is already proposed in literature [30]. Then the primary discharge would form an unstable intermediate OH^* , which further convert into more stable OH .



The observed Tafel slope of 64 mV supports the above mentioned mechanism with a reaction order around -1, which also resembles with the actual reaction order value we got experimentally.

4. CONCLUSIONS

In the present study, tin-doped hollow carbon sphere electrocatalysts were synthesized using polystyrene (PSs) as template materials along with the glucose decomposition in a poly(ethylene glycol)-block-poly(propylene glycol)-block-poly(ethylene glycol) (P123) surfactant containing

solution under hydrothermal condition using an intermittent microwave heating (IMH) technique. The addition P123 has created huge amount of pores over the spherical surface, and also increase the pore size, resulted in the ultrahigh surface area of $1300 \text{ m}^2 \text{ g}^{-1}$. After tin loading over the spheres, the pores were blocked to some extent resulting in the reduced surface area values, although the values are sufficiently large to exhibit good electrocatalytic activity in hydrogen and oxygen production from water electrolysis. N_2 adsorption isotherms have exhibited typical type – I of microporous materials. The XRD studies have confirmed the presence of rutile SnO_2 phase in the electrocatalysts; whereas SEM and TEM images of materials have assured the spherical structure formation of the materials with the diameter of 300 – 400 nm. The micrographs also confirmed the SnO_2 formation over the spherical structures. The electrocatalytic activity of Sn-doped HCS materials have greatly enhanced in hydrogen and oxygen evolution reaction, in comparison with the HCS – 6. The great H_2 adsorption characteristic and oxygen deficiency of SnO_2 structure has influenced the significant increase in the electrocatalytic activity of Sn-doped materials. Among all the electrocatalysts, 30 wt% Sn/HCS – 6 has shown the best electrocatalytic activity with 30 and 50 mA.cm^{-2} of cathodic and anodic peak current density value, respectively. The reaction mechanism of the water electrolysis system has exhibited the average reaction order value of -1.16 with Tafel slope of 64 mV.

ACKNOWLEDGEMENT

This research work has been funded by SERC, Department of Science and Technology, New Delhi under Fast Track Young Scientist Scheme. We are thankful to SERC-DST for the financial assistant.

References

1. B. Børresen, G. Hagen and R. Tunold, *Electrochim. Acta*, 47 (2002) 1819.
2. R. Davies, G. A. Schurr, P. Meenan, R. D. Nelson, H. E. Bergna, C. A. S. Brevett and R. H. Goldbaum, *Adv. Mater.*, 10 (1998) 1264.
3. F. Caruso, *Adv. Mater.*, 13 (2001) 11.
4. J. Lee, J. C. Park and H. Song, *Adv. Mater.*, 20 (2008) 1523.
5. I. Gill and A. Ballesteros, *J. Am. Chem. Soc.*, 120 (1998) 8587.
6. D. Lee, M. F. Rubner and R. E. Cohen, *Chem. Mater.*, 17 (2005) 1099.
7. E. Mathiowitz, J. S. Jacob, Y. S. Jong, G. P. Carino, D. E. Chickering, P. Chaturvedi, C. A. Santos, K. Vijayaraghavan, S. Montgomery, M. Bassett and C. Morrell, *Nature*, 386 (1997) 410.
8. H. Huang, E. E. Remsen, T. Kowalewski and K. L. Wooley, *J. Am. Chem. Soc.*, 121 (1999) 3805.
9. Y. Yin and A. P. Alivisatos, *Nature*, 437 (2005) 664.
10. H. W. Kroto, *Nature*, 359 (1992) 670.
11. Y. Xiao, Y. Liu, L. Cheng, D. Yuan, J. Zhang, Y. Gu and G. Sun, *Carbon*, 44 (2006) 1589.
12. Y. Xiao, Y. Liu, Y. Mi, D. S. Yuan, *Chem. Lett.*, 34 (2005) 1422.
13. G. F. Zou, J. Lu, D. B. Wang, L. Xu and Qian Y, *Inorg. Chem.*, 43 (2004) 5432.
14. Z. Wen, Q. Wang, Q. Zhang and J. H. Li, *Electrochem. Comm.*, 9 (2008) 1867.
15. G. Hu, D. Ma, M. Cheng, L. Liu and X. Bao, *Chem. Comm.*, 17 (2002) 1948.
16. L. Q. Xu, W. G. Zhang, Q. Yang, Y. W. Ding, W. C. Yu and Y. T. Qian, *Carbon*, 43 (2005) 1090.
17. J. W. Liu, M. W. Shao, Q. Tang, X. Y. Chen, Z. P. Liu and Y. T. Qian, *Carbon*, 41 (2003) 1682.
18. X. G. Yang, C. Li, W. Wang, B. J. Yang, S. Y. Zhang, Y. T. Qian, *Chem. Comm.*, 3 (2004) 342.
19. J. Wu, F. Hu, X. Hu, Z. Wei and P. K. Shen, *Electrochimica Acta*, 53 (2008) 8341.
20. J. Chattopadhyay, H. R. Kim, S. B. Moon and P. Daewon, *Int. J. Hydrogen Energy*, 33 (2008) 3270.

21. W. M. Zhang, J. S. Hu, Y. G. Guo, S. F. Zheng, L. S. Zhong, W. G. Song and L. J. Wan, *Adv. Mater.*, 20 (2008) 1160.
22. P. M. Tessier, O. D. Velev, A. T. Kalambur, A. M. Lenhoff, J. F. Rabolt and E. W. Kaler, *Adv. Mater.*, 13 (2001) 396.
23. X. Chen, G. Chen and P. Yue, *J. Phys. Chem. B*, 105 (2001) 4623.
24. S. Ardizzone, C. Bianchi, G. Cappelletti, M. Ionita, A. Minguzzi and S. Rondinini, *J. Electroanal. Chem.*, 589 (2006) 160.
25. Y. Liang, J. Fan, X. Xia and Z. Jia, *Mater. Lett.* 61 (2007) 4370.
26. Woods R. In: Bard A, editor. *Chemisorption at electrodes in electroanalytical chemistry*, vol. 9. New York: Marcel Dekker; 1976.
27. I. Garcí'a, M. Torres, M. Crespo, C. Rodrí'guez and E. Estrada, *J. Alloy Comp.*, 434 (2007) 764.
28. P. Giannozzi, R. Car and G. Scoles, *J. Chem. Phys.*, 118 (2003) 1003.
29. M. Batzill and U. Diebold, *Prog. Surf. Sci.*, 79 (2005) 47.
30. A. Hrussanova, E. Guerrini, S. Trasatti, *J. Electroanal. Chem.* 564 (2004) 151.